ChemPubSoc Europe

DOI: 10.1002/chem.201600178

CHEMISTRY A European Journal Full Paper

Molecular Switches

Multistate Switches: Ruthenium Alkynyl–Dihydroazulene/Vinylheptafulvene Conjugates

Alexandru Vlasceanu, Cecilie L. Andersen, Christian R. Parker, Ole Hammerich, Thorbjørn J. Morsing, Martyn Jevric, Søren Lindbæk Broman, Anders Kadziola, and Mogens Brøndsted Nielsen*[a]

Abstract: Multimode molecular switches incorporating distinct and independently addressable functional components have potential applications as advanced switches and logic gates for molecular electronics and memory storage devices. Herein, we describe the synthesis and characterization of four switches based on the dihydroazulene/vinylheptafulvene (DHA/VHF) photo/thermoswitch pair functionalized with the ruthenium-based Cp*(dppe)Ru ([Ru*]) metal complex (dppe = 1,2-bis(diphenylphosphino)ethane; Cp* = pentamethylcyclopentadienyl). The [Ru*]–DHA conjugates can potentially exist in six different states accessible by alternation between DHA/VHF, Ru^{II}/Ru^{III}, and alkynyl/vinylidene, which can be individually stimulated by using light/heat, oxidation/reduction, and acid/base. Access to the full range of states was found to be strongly dependent on the electronic communication between the metal center and the organic photoswitch in these [Ru*]–DHA conjugates. Detailed electrochemical, spectroscopic (UV/Vis, IR, NMR), and X-ray crystallographic studies indeed reveal significant electronic interactions between the two moieties. When in direct conjugation, the ruthenium metal center was found to quench the photochemical ring-opening of DHA, which in one case could be restored by protonation or oxidation, allowing conversion to the VHF state.

Introduction

Molecular switches play a key role in the development of functional molecular electronics devices.[1] In this way, conventional computing operations could potentially be performed by single molecules functioning as transistors or logic gates.[2] In addition, the development of compounds that can exist in multiple states, exhibiting distinct optical properties, interconvertible by external stimuli has become a research forefront with considerable prospects in this field.[3] One strategy towards multistate molecules is through the combination of distinct functional components such as redox-active, photoactive, or pH-responsive groups.[4] This can be achieved through the functionalization of organic molecular switches with organometallic moieties, as has been recently reviewed by Akita.[5] With regard to this, Ru^{II} acetylides have been extensively studied in the literature due to their favorable properties.[6] The strong electron-donating properties of the Ru^{II} metal center in such complexes can typically be modulated by either reversible oxidation to the Ru^{III} species or protonation to the corresponding vinylidene. This has been used in the formation of dithienylethene (DTE) photoswitches end-capped with ruthenium alkynyl groups such as *trans*-$(dppe)_2RuX$[7] or Cp*(dppe)Ru[8] producing multistate systems (dppe = 1,2-bis(diphenylphosphino)ethane, Cp* = pentamethylcyclopentadienyl anion). The proximity of the Ru metal center to the thiophene ring was observed to influence the switching behavior and impart properties unlike those observed for related Fe complexes.[8a] Effective radical delocalization into the DTE photochromic system could be suppressed by using a phenylene spacer, thus allowing for the preparation of a multimode switch exhibiting six states with distinct non-linear optical (NLO) properties, independently interconvertible by acid/base (alkynyl versus vinylidene ligand), electrochemical (Ru^{II} versus Ru^{III}), and light (ring-opening/closure) stimulation.[9] The incorporation of ruthenium alkynyl moieties was also shown to modulate the coupling between gold electrodes and a central DTE unit when one such molecule was suspended between two electrodes by anchoring to sulfur end-groups. In this case, the ruthenium complexes prevented quenching of the DTE photoswitching by the electrodes.[4,10]

It has recently been shown that suitably functionalized dihydroazulene (DHA, **1A**)/vinylheptafulvene (VHF, **1D**) photo/thermoswitches (Scheme 1) can also undergo light- and heat-controlled conductance modulation in molecular junctions.[11] Additionally, the incorporation of various functional components as well as donor and/or acceptor groups through conjugated or non-conjugated bridges into the DHA/VHF system has pre-

[a] A. Vlasceanu, C. L. Andersen, Dr. C. R. Parker, Prof. Dr. O. Hammerich, Dr. T. J. Morsing, Dr. M. Jevric, Dr. S. Lindbæk Broman, Prof. Dr. A. Kadziola, Prof. Dr. M. B. Nielsen
Department of Chemistry and Center for Exploitation of Solar Energy
University of Copenhagen, Universitetsparken 5
2100 Copenhagen (Denmark)
E-mail: mbn@chem.ku.dk

Supporting information and ORCIDs from the authors for this article are available on the WWW under http://dx.doi.org/10.1002/chem.201600178.

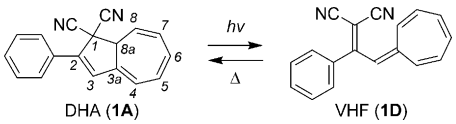

Scheme 1. DHA/VHF interconversion and DHA atom numbering.

sented a way to tune both the light-induced ring-opening of DHA and the thermal ring-closure of VHF.[12]

To take advantage of multiple functional groups and expand the scope of the DHA/VHF system, functionalization with Ru^{II} alkynyl groups, based on Cp*(dppe)Ru ([Ru*]) complexes, was undertaken. Herein, we describe the synthesis, characterization, and multimode switching behavior of four bridged [Ru*]–DHA conjugates (**2A**–**5A**) shown in Figure 1. The position of the

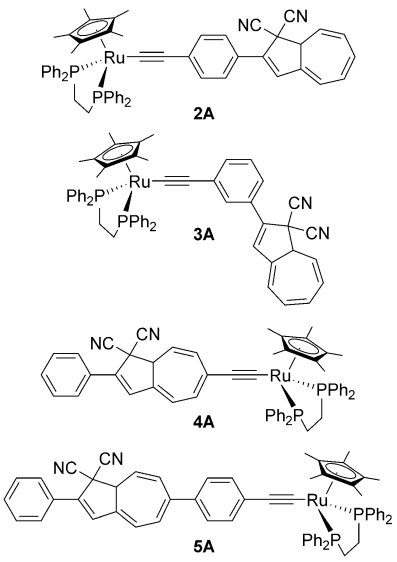

Figure 1. [Ru*]–DHA conjugates **2A**–**5A**.

[Ru*] acetylide functionality, either *meta* or *para* on the phenylene ring to the DHA core (**2A** and **3A**), at the DHA 6-position with direct attachment (**4A**), or with a *p*-phenylene spacer (**5A**) was found to strongly influence the properties of the system. The proposed switching behavior of a [Ru*]–DHA complex is shown in Scheme 2, which shows that the system can reach six different states including two neutral (**A**/**D**), two vinylidene (**B**/**C**), and two dimeric (**F**/**E**) forms, interchangeable by a combination of light/heat, oxidation/reduction, and acid/base stimulation. The latter, dimeric states (**F**/**E**), are tentatively assigned as the result of redox stimulation, which is discussed in more detail below.

Results and Discussion

Synthesis

The coupling between the ruthenium and DHA moieties of conjugates **2A**–**5A** was undertaken via two methods: i) by a metalation approach,[13] using Cp*(dppe)RuCl and an ethynyl-

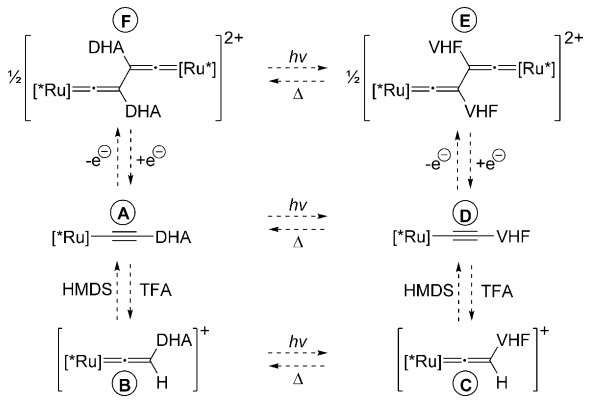

Scheme 2. Conversion between the six states of a [Ru*]–DHA complex.

functionalized DHA proceeding via a vinylidene intermediate, which is subsequently deprotonated, and ii) by Sonogashira cross-coupling[13b,14] between Cp*(dppe)RuC_2H and a halide-functionalized DHA (Scheme 3). The two protocols encompass

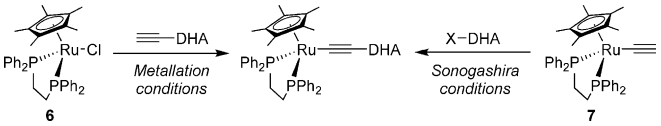

Scheme 3. Metalation and Sonogashira cross-coupling protocols for assembling the [Ru*]–DHA conjugates. X = halogen.

both possibilities for forming either the [Ru*]–alkynyl or alkynyl–DHA bond in the final step. The two ruthenium precursors **6** and **7** were readily prepared according to known procedures[15] as were the two iodo-functionalized DHAs **8** and **9** (Figure 2),[12d,16] which are precursors for **2A** and **3A**. Ethynyl-functionalized DHAs **10** and **11** were prepared by following a strategy starting from alkyne-functionalized acetophenone derivatives described in the Supporting Information (Section 2) and similar to previous reports.[12j,16] DHAs **12** and **13** (precursors for **4A** and **5A**) were prepared from **1A** (readily obtained on a large scale[17]) by employing a bromination/elimination/cross-coupling strategy.[12f,g,h,18] An isomerization reaction in the synthesis of **4A** and **5A** occurred under the metalation conditions (see below).

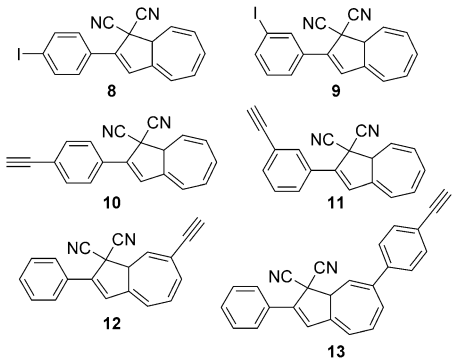

Figure 2. DHA building blocks.

The successful preparation of **2A** and **3A** by the two different routes is shown in Scheme 4. It was found that the metalation of ethynyl DHAs required elevated temperatures overnight to reach completion, whereas simpler literature-reported substrates, for example, phenylacetylene, could be metalated

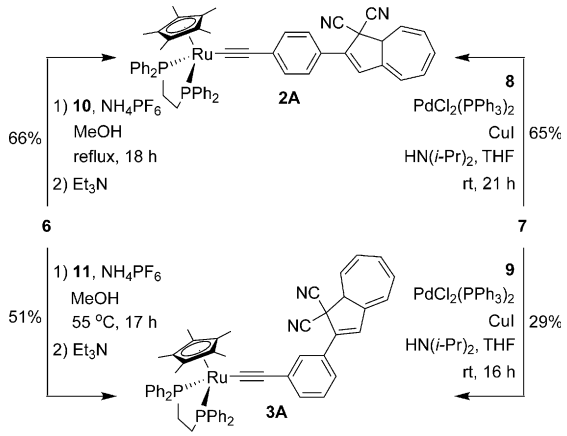

Scheme 4. Synthesis of [Ru*]–DHA conjugates **2A** and **3A**.

within 1 h.[13a] This may occur as a result of competitive, yet reversible, coordination of the nitrile groups of DHA to the $[Cp^*(dppe)Ru]^+$ metal complex. The displacement of chloride from Cp*(dppe)RuCl in favor of MeCN coordination, promoted by NH_4PF_6 in MeOH, has been reported to yield $[Cp^*(dppe)Ru(MeCN)]PF_6$, which exhibits a characteristic singlet in the ^{31}P NMR (CD_2Cl_2) spectrum at $\delta = 75.52$ ppm.[19] The combination of Cp*(dppe)RuCl (**6**) with **1A** under analogous conditions leads to a reaction mixture from which a yellow/green solid can be isolated. The ^{31}P NMR (CD_2Cl_2) spectrum of this product includes an AB system, $\delta = 75.37$ (d, $J = 20.1$ Hz), 76.02 ppm (d, $J = 20.1$ Hz) as well as a singlet ($\delta = 75.97$ ppm), which likely correspond to a diastereoisomeric mixture of $[Cp^*(dppe)Ru(DHA)]PF_6$ salts.

The syntheses of **4A** and **5A** were accomplished via the metalation strategy by combining **6** with **12** and **13**, respectively (Scheme 5). Interestingly, both reactions proceeded through an isomerization by which the ruthenium–alkynyl substituent shifted from position 7 to position 6 on the DHA core. Partial 7/6-isomerization has previously been observed as

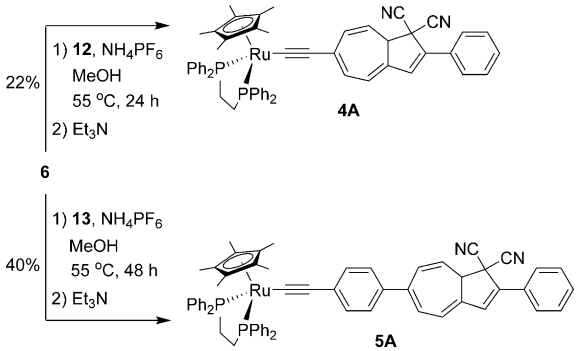

Scheme 5. Synthesis of [Ru*]–DHA conjugates **4A** and **5A**.

a result of a light–heat cycle (ring-opening/ring-closure), yielding mixtures of the two isomers.[12g,h] In the present case, however, the isomerization does not involve irradiation. Such a process has been previously noted in a sterically strained DHA whereby a substituent shift was observed to occur from the 8- to the 5-position in the absence of photochemical stimulation.[12i] To test the possibility of isomerization in the absence of Ru, DHA **12** was submitted to overnight reflux in NH_4PF_6/MeOH but no signs of any reaction or isomerization were seen. To further investigate the nature of this phenomenon, the metalation reaction between **6** and **12** was interrupted before deprotonation, allowing for the isolation of the 6-substituted vinylidene intermediate (**14**; Scheme 6). No evidence of any 7-substituted derivative could be found. Treatment of **14** with NEt_3 gave product **4A**, which could be protonated by trifluoroacetic acid (TFA) to generate the trifluoroacetate salt of **14** (**4B**), confirmed by ^1H-^1H COSY NMR spectroscopy.

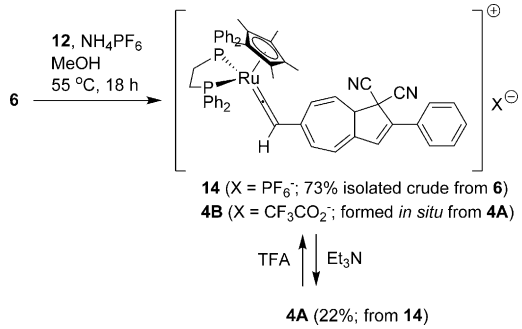

Scheme 6. Trapping the 6-substituted vinylidene intermediate (**14**).

From the reaction mixture obtained through the coupling of **6** and **12**, several interesting [Ru*]–DHA and [Ru*]–azulene byproducts were isolated during column chromatographic purification (Figure 3). Azulene **15** and furoazulene **16** were both

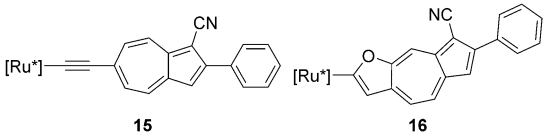

Figure 3. Byproducts from the metalation reaction between **6** and **12**.

characterized, the latter also by X-ray crystallography (see below). The formation of **16** might be a result of nucleophilic attack by residual water at the susceptible α-carbon of vinylidene **14**, which subsequently undergoes cyclization with the cycloheptatriene ring. Such nucleophilic attack has more often been observed for less bulky Ru complexes.[20] The presence of the O atom at the 7-position of compound **16** suggests that the vinylidene had already isomerized to the 6-position before the nucleophilic attack by water took place. The azulene moieties of **15** and **16** are most likely formed as a result of HCN elimination, a phenomenon commonly observed in DHA synthesis.[16]

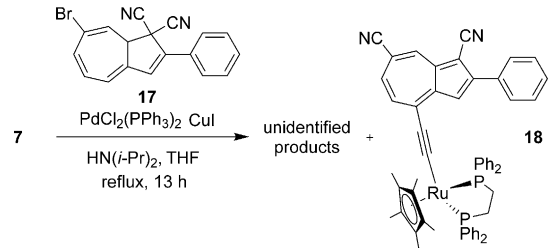

Scheme 7. Sonogashira reaction between **7** and **17**, which gave, among other unidentifiable products, minute quantities of azulene **18**.

A Sonogashira reaction between **7** and 7-bromo-substituted DHA **17** was also attempted (Scheme 7). Although no evidence of the desired product was found, column chromatographic purification of the crude mixture revealed a variety of products. Among these, X-ray crystallography (see below) revealed one complex that could be assigned to the azulene structure **18** in which the alkyne substituent has moved to position 4 and a cyano group has been incorporated at position 7, alluding to more complex reactions.

Characterization

Key to the potential of multimode switches in molecular electronics devices is the electronic communication between the different functional components of the system. Here, we partially describe the geometric (X-ray crystallographic), spectroscopic (NMR, IR, UV/Vis), and electrochemical characteristics of [Ru*]–DHA dyads **2A**–**5A** in their neutral (**A**/**D**), vinylidene (**B**/**C**), and oxidized (**F**/**E**) forms. Vinylidine analogs **2B**–**5B** could all be quantitatively formed in situ by treatment of **2A**–**5A** with TFA (see the Supporting Information, Section 2). Characterization data for literature-reported complexes **19**–**23**[13b,21] (Figure 5) are also reported here as references for comparison.

Single-crystal X-ray crystallography was used to reveal the structures of [Ru*]–DHA conjugates **2A** and **4A**, which are shown in Figure 4. Table 1 lists selected bond lengths in comparison to parent DHA **1A**[17] and ruthenium complexes **19**–**21**.[13b] Longer C≡C triple bonds are observed in the [Ru*]–DHA conjugates relative to the uncomplexed DHA–alkynes (**10**, **11**, and **13**), which is indicative of partial electronic communication with the metal center. The molecular structures of azulene byproducts **16** and **18** are shown in Figure 6.

Electrochemistry was used to determine the standard redox potentials of all [Ru*]–DHA conjugates both in the acetylide (**2A**–**5A**) and vinylidene (**2B**–**5B**) forms. Cyclic voltammograms (CVs) were acquired between approximately −2 and +1 V and, for **2A**–**5A**, were found to exhibit electrochemically reversible oxidation waves at approximately −0.2 V versus Fc/Fc$^+$, corresponding to the Ru^{II}/Ru^{III} redox event (Table 2). As expected, these potentials are comparable to those for **19**–**23**. The re-

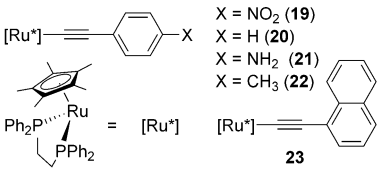

Figure 5. Reference complexes Cp*(dppe)RuC$_2$PhX (**19**–**21**)[13b] and **22**–**23**.[21]

Table 1. Selected bond lengths (crystallographic data).[a]

	[Ru*]–C [Å]	C≡C [Å]	C_{alkyne}–C_X[b] [Å]	C1–C8a [Å]
1A[c]	–	–	–	1.575(1)
10	–	1.201(3)	1.432(3)	1.584(2)
		1.191(3)	1.448(3)	1.572(7)
11	–	1.179(4)	1.440(3)	1.580(3)
		1.182(3)	1.441(3)	1.577(3)
13	–	1.180(3)	1.441(3)	1.569(2)
2A	2.005(2)	1.218(4)	1.433(4)	1.595(5)
4A	1.979(3)	1.220(5)	1.421(5)	1.582(7)
16	2.031(2)	1.393(4)[d]	1.414(3)	1.420(3)
18	1.960(4)	1.212(6)	1.407(6)	1.416(5)
19[e]	1.997(6)	1.221(8)	1.437(8)	–
	2.004(6)	1.225(8)	1.413(8)	
20[e]	2.011(4)	1.215(5)	1.431(5)	–
21[e]	2.026(3)	1.202(4)	1.444(4)	–

[a] When more than one molecule is present in the asymmetric unit, the length of the indicated bond is reported for each molecule. [b] X = DHA, Ar, or azulene. [c] Ref. [17]. [d] Bond length corresponding to [Ru*]-C≡C of the furan ring. [e] Ref. [13b].

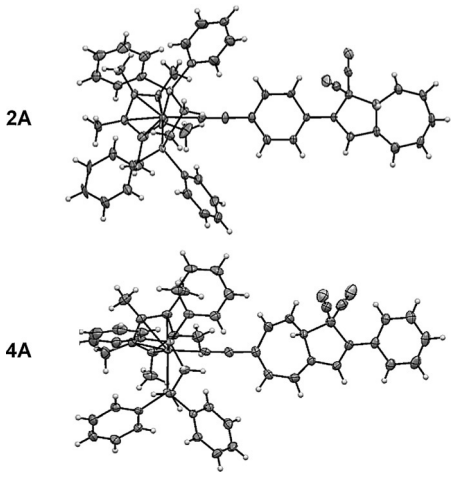

Figure 4. Molecular structures of **2A** and **4A** with displacement ellipsoids drawn at the 50% probability level for non-hydrogen atoms.

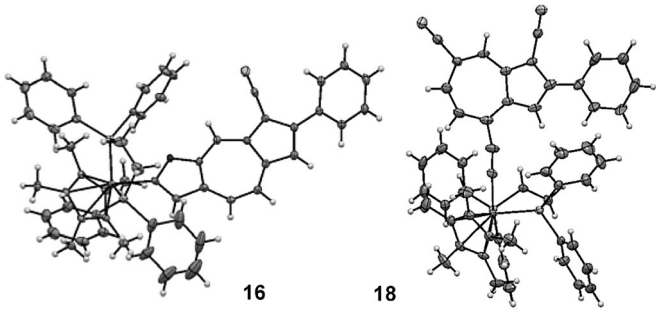

Figure 6. Molecular structures of **16** (left) and **18** (right).

Table 2. Cyclic voltammetry data.[a]

Complex	$E^o(1)$[b] [V]	ΔE_p[c] [V]	i_{pc}/i_{pa}[d]	$E_p(2)$[e] [V]	$E_p(1)$[f] [V]
2A	−0.17	0.06	>0.90	0.68	
2B					0.76
3A	−0.18	0.06	>0.95	0.72	
3B					0.86
4A	−0.22	0.07	>0.90	0.55	
4B					0.52
5A	−0.21	0.08	>0.93	0.65	
5B					0.62
19[g]	−0.06	0.09	>0.95		
20[g]	−0.23	0.09	>0.90		
21[g]	−0.41	0.09	>0.85	0.13	
22[h]	−0.15	0.09	1.0	0.71	
23[h]	−0.10	0.11	1.0	0.82	

[a] Obtained at a glassy carbon working electrode, at room temperature, using 0.5 mM [Ru*]–DHA (see the Supporting Information, Section 4.2) and 0.1 M Bu_4NPF_6 supporting electrolyte in CH_2Cl_2, at a sweep rate of 0.1 V s^{-1}. Potentials are given versus the ferrocene/ferrocenium redox couple (Fc/Fc^+). [b] Formal oxidation potential for the first reversible one-electron oxidation taken as $(E_{pa}+E_{pc})/2$. [c] Peak separation of $E^o(1)$ taken as $|E_{pa}-E_{pc}|$. [d] Peak current ratio of $E^o(1)$. [e] Peak potential for the second, irreversible oxidation event. [f] Peak potential for the first, irreversible oxidation of complexes **2B**–**5B**. [g] From Ref. [13b]; recorded at 20 °C at a Pt working electrode. The formal oxidation potentials have been converted by the present authors to the Fc/Fc^+ scale by subtraction of 0.460 V. [h] From Ref. [21]; recorded at 20 °C at a Pt working electrode. The formal oxidation potentials have been converted by the present authors to the Fc/Fc^+ scale by subtraction of 0.460 V.

sults indicate that **4A** and **5A** are marginally easier to oxidize than **2A** and **3A**, which is not surprising as the [Ru*]–acetylide moiety is attached to the partially electron-donating seven-membered ring. A second, irreversible oxidation can be observed at approximately +0.6 V for **2A**–**5A** as was also observed for reference complexes **22**–**23**.

The reversibility of the **2A** oxidation was found to be dependent on the concentration of the sample, providing strong evidence for a second-order intermolecular dimerization (Table 3). The reaction was observed to occur on the second/minute timescale for **2A**, which displays scan-rate-dependent i_{pc}/i_{pa} reversibilities. Electrolysis of all complexes **2A**–**5A** resulted in a chemical event (but not corresponding to dimerization for **3A**–**5A**, see below) that quantitatively consumed the transient Ru^{III} species, giving rise to indicative color changes.

Table 3. Concentration (c) and sweep rate (ν) dependence of the CV peak current ratio, i_{pc}/i_{pa}, for the Ru^{II}/Ru^{III} redox couple of complex **2A**.[a]

c [mM]	i_{pc}/i_{pa} (ν = 0.05 V s^{-1})	i_{pc}/i_{pa} (ν = 0.1 V s^{-1})	i_{pc}/i_{pa} (ν = 0.2 V s^{-1})	i_{pc}/i_{pa} (ν = 0.5 V s^{-1})
4.6	0.84	0.90	0.95	0.99
2.3	0.92	0.95	0.98	0.99
1.15	0.95	0.98	0.99	1.00
0.58	0.98	0.99	1.00	1.00
0.29	1.00	1.00	1.00	0.99

[a] Recorded at a glassy carbon working electrode (d = 3 mm) in CH_2Cl_2 with 0.1 M Bu_4NPF_6 as supporting electrolyte.

It is hypothesized that the initial oxidations of Ru^{II}–DHA complexes **2A**–**5A** lead to significantly delocalized Ru^{III} radical cations, which undergo further chemical reactions and are thus not observed on the timescale of the spectroscopic experiments conducted here. The fleeting stability of such Ru^{III} complexes is well-established in the literature. For analogous metal complexes, experimental observations, supported by calculations, have identified C_β of the alkynyl moiety as a site very prone to further reactivity.[21–24] Thus, one possible explanation for the chemical reaction observed here, resulting from the oxidation of **2A**, could be that of a C_β–C_β radical dimerization between two oxidized [Ru*]–DHA species. A more detailed investigation into the oxidative dimerization products of $Cp(PPh_3)_2RuC_2Ph$ with $[FeCp_2]PF_6$ was recently undertaken by Bruce et al.[22g] Solvent-dependent redox chemistry in an analogous oxidation using Ag^I salts on $Cp(PPh_3)_2RuC_2Ph$ was also explored, in one case leading to the isolation of divinylidene $[\{Cp(PPh_3)_2Ru\}_2(\mu\text{-}C_4Ph_2)][PF_6]_2$.[23] In other trials, oxidations of $Cp^*(dppe)RuC_2PhX$ using AgOTf also resulted in unstable radical cations leading to more complex product mixtures.[13b] Such behavior, however, was not observed for the analogous Fe derivatives, the oxidized states of which show greater stability.[24] This is thought to be the result of a more localized and shielded, metal-centered Fe^{III} radical.

The chemical process following the oxidation of **2A** was further investigated by conducting bulk electrolysis of this complex. The electrochemical experiment was monitored by cyclic voltammetry and found to result in complete consumption of **2A**, consistently leading to the quantitative formation of a single, bright-yellow product (**2F**). Subjecting **2A** to chemical oxidation by using AgOTf or $[FeCp_2]PF_6$, however, resulted in a more complex mixture of **2F** and other products, not investigated further. Thus, the clean and quantitative formation of **2F**, from **2A**, could only be achieved by electrochemical means and, although **2F** was observed to be particularly stable in the electrolytic medium (0.1 M Bu_4NPF_6 in CH_2Cl_2 or CD_2Cl_2), standard purification techniques were unsuccessful in isolating the pure complex. Bulk electrolysis of **2A** in CD_2Cl_2 (see the Supporting Information, Section 5) allowed for detailed spectroscopic (^1H, ^{13}C, ^{31}P NMR, IR, and UV/Vis) characterization in situ. Furthermore, the oxidative dimerization of **2A** to **2F** was found to be readily reversible by reduction, almost quantitatively regenerating starting material **2A**. This interconversion could reliably be followed by UV/Vis spectroelectrochemical experiments (see below) as well as by cyclic voltammetry over the course of bulk electrolytic experiments. The latter also provided ^1H and ^{31}P NMR spectroscopic evidence of a clean reductive fragmentation from **2F** back to **2A**.

Analogous electrochemical oxidations of **3A**–**5A**, however, were not found to furnish similar oxidation products (**3F**–**5F**), as observed for **2A**. These were instead, quite surprisingly, identified by NMR spectroscopy as the vinylidene species **3B**–**5B** (see the Supporting Information, Section 5). Although this redox process was also found to be reversible, regenerating the **A** species (see the Supporting Information, Section 4), the mechanistic details of the electrochemical interconversion between **3A**–**5A** and **3B**–**5B** could not be elucidated further.

Table 4. Selected ^{13}C and ^{31}P NMR spectroscopic data.[a]

	Solvent	[Ru*]–*C*–C δ_C [ppm]	dppe δ_P [ppm]
2A	C_6D_6	140.22 (t, $^2J_{CP}$ = 24.5 Hz)	81.36 (s)
	CD_2Cl_2	n.o.	81.14 (s)
2B	C_6D_6	353.14 (t, $^2J_{CP}$ = 15.9 Hz)	72.37 (s)
	CD_2Cl_2	n.o.	72.59 (s)
2F[b]	CD_2Cl_2	n.o.	72.26 (s)
3A	C_6D_6	133.23 (t, $^2J_{CP}$ = 24.6 Hz)	81.69 (d, $^2J_{PP}$ = 13.9 Hz)
			81.56 (d, $^2J_{PP}$ = 13.9 Hz)
3B	C_6D_6	349.93 (t, $^2J_{CP}$ = 16.1 Hz)	72.90 (s)
4A	C_6D_6	142.66 (t, $^2J_{CP}$ = 24.7 Hz)	81.52 (d, $^2J_{PP}$ = 14.7 Hz)
			81.28 (d, $^2J_{PP}$ = 14.7 Hz)
4B	C_6D_6	355.14 (t, $^2J_{CP}$ = 16.2 Hz)	72.67 (d, $^2J_{PP}$ = 19.6 Hz)
			72.05 (d, $^2J_{PP}$ = 19.6 Hz)
5A	C_6D_6	n.o.	81.71 (d, $^2J_{PP}$ = 13.9 Hz)
			81.51 (d, $^2J_{PP}$ = 13.9 Hz)
5B	C_6D_6	354.07 (t, $^2J_{CP}$ = 16.1 Hz)	72.87 (s)
15	C_6D_6	136.40 (t, $^2J_{CP}$ = 25.0 Hz)	81.03 (s)
		164.25 (t, $^2J_{CP}$ = 23.9 Hz)	

[a] n.o. = not observed. [b] Complex **2F** was characterized as the crude product obtained from the electrolysis experiment in 0.1 M Bu_4NPF_6/CD_2Cl_2 (see the Supporting Information, p. S7). [c] Ref. [13b]. [d] Ref. [21].

NMR spectroscopy revealed characteristic signals of which selected data are provided in Table 4. Conjugates **2A**–**5A** all present expected ^{31}P NMR signals near 81 ppm, corresponding to the two phosphorous atoms of the dppe ligand, analogous to those observed for reference complexes **19**–**23**[13b,21] ($CDCl_3$, δ = 81.1–82.5). The two P nuclei of the [Ru*]–DHA conjugates are inherently diastereotopic because of the stereocenter at C8a of the DHA unit, which thus explains the AB doublets observed for complexes **3A**, **4A**, and **5A** in C_6D_6. The ^{31}P NMR spectrum of complex **2A**, however, exhibits only a singlet, suggesting that the chiral environment is not as strongly felt by the two phosphorus nuclei. The ^{13}C NMR spectra of **2A**–**5A** exhibit the expected triplet resonances, characteristic of the α-acetylide carbon atoms, near 140 ppm, with coupling constants of approximately $^2J_{CP}$ = 25 Hz. In comparison, vinylidene analogs **2B**–**5B** all present strongly downfield-shifted ^{13}C triplets near δ = 350 ppm for the α-carbon of vinylidene, upfield-shifted ^{31}P NMR resonances around δ = 72 ppm, as well as a β-^1H singlets near δ = 4.5 ppm. Notably, the ^{31}P NMR resonances are observed as singlets for complexes **3B** and **5B** in contrast to the pair of AB doublets observed for acetylides **3A** and **5A** in C_6D_6.

Complex **2F**, the oxidation product of **2A**, was obtained and spectroscopically characterized as the crude product of electrolysis experiments in 0.1 M Bu_4NPF_6/CD_2Cl_2. The ^{31}P NMR spectrum of **2F** presents a sharp singlet at δ = 72.23 ppm, similar to vinylidene **2B** at δ = 72.59 ppm. Complex **2A** was found to be notably sensitive to its surroundings. Although relatively stable in C_6D_6 and neutralized CD_2Cl_2, any residual acid in a solution of the latter resulted in a delicate equilibrium arising between the neutral (**2A**), vinylidene (**2B**), and oxidized (**2F**) states, which varied according to the specific conditions. Figures S66 and S67 (in the Supporting Information, p. S100) show ^1H and ^{31}P NMR spectra of a mixture of these three species, thereby supporting their individual identities.

IR spectroscopy also provides strong evidence for electronic communication between the DHA and the Ru metal center, which acts as a strong electron donor. As expected, lower energy C≡C stretches in the IR region are observed for conjugates **2A**–**5A** at approximately 2050 cm^{-1}, similar to those of **19**–**23** (2041–2073 cm^{-1}),[13b,21] in comparison to the trialkylsilyl-terminated derivatives of **10**, **11**, and **13** at approximately 2150 cm^{-1} (Table 5). The C≡N stretching vibrations were found at higher energies. The C≡C stretching vibrations of the free alkynes (**10**–**13**) could not be observed. Vinylidene derivatives **2B**–**5B** exhibited characteristic IR absorptions in the region 1700–1800 cm^{-1}. Notably, literature investigations reveal that the Ru^{III} radical cations of reference complexes **20** and **22**–**23** all show C≡C stretching vibrations at approximately 1920 cm^{-1}. The absence of such a signal in the spectrum of **2F** indicates the absence of a Ru^{III} acetylide motif. The presence of a stretch at 1708 cm^{-1}, however, supports a vinylidene-like structure for this complex.

UV/Vis absorption spectroscopy of the [Ru*]–DHA conjugates reveals characteristic DHA absorptions at approximately 350 nm (Table 6). Higher energy shoulders near 250 nm are found for all compounds including **2A**–**5A** (Figure 7), parent DHA **1A**, and reference complexes **19**–**23**.[13b,21] Similar to these references, [Ru*]–DHA conjugates **2A**–**5A** also exhibit lower energy absorptions in the region between 300 and 500 nm. For **19**–**21**, Paul et al.[13b] have attributed these transitions to metal-to-ligand charge-transfer (MLCT) bands based on analogy with the Fe analogs.[24] Spectroelectrochemical UV/Vis/NIR studies of **20** and **22**–**23** by Fox et al.[21] have revealed that the absorption bands in this region are increasingly red-shifted with the increasing size of the aromatic ligand. Time-dependent density functional theory (TD-DFT) calculations on **20**, **22**, and **23** have likened the origin of these transitions to (d/π)–phenyl π^* charge-transfer bands (HOMO→[LUMO + 3]) rather than purely MLCT bands. The absorptions exhibited by **2A**–**5A** in this region are thus hypothesized to arise from

Table 5. Selected IR absorptions (ATR, neat).[a]

	ν(C≡C) or ν(C=C) [cm^{-1}]	ν(C≡CN) [cm^{-1}]
1A	–	2244 (vw)
10-$SiMe_3$[b]	2155 (s)	2249 (w)
11-Si(*i*Pr)$_3$[b]	2156 (w)	2254 (w)
13-Si(*i*Pr)$_3$[b]	2154 (m)	2246 (w)
2A	2053 (s)	n.o.
2B	1780 (m), 1717 (m)	n.o.
2F[c]	1708 (m)	n.o.
3A	2057 (s)	n.o.
3B	1781 (m), 1717 (m)	n.o.
4A	2035 (s)	2279 (w)
4B	1782 (m), 1717 (m)	n.o.
5A	2064 (s)	2279 (w)
5B	1781 (m), 1716 (m)	n.o.
15	2008 (s)	2194 (w)

[a] Relative signal intensity: vs = very strong, s = strong, m = medium, w = weak, vw = very weak. n.o. = not observed. [b] Trialkylsilyl-terminated alkyne. [c] The complex was deposited as a thin film by evaporation from a 0.1 M solution of Bu_4NPF_6 in CD_2Cl_2 obtained from electrolysis experiments.

Table 6. Selected UV/Vis absorption maxima (λ_{max} [nm]) associated with **1A/D**, the different states of [Ru*]–DHA conjugates **2A**–**5A**, and reference complexes **19**–**23**. Where available, values are reported in MeCN and/or approximately 0.1 M Bu_4NPF_6/CH_2Cl_2.[a]

	A[b]	B	C	D	E	F[b]
1	(353) 357	–	–	(470) 475	–	–
	–	–	–	(345) 328	–	–
2	(348) 402	(398)	(465)	(474) 474	470	396
	(472) 480	–	–	(600) 600	–	–
3	–	–	–	(332) 336	–	–
	(356) 358	(356) 358	(478) 480	(474) 474	–	–
4	(328) 334	(430) 428	–	–	–	–
	(522) 528	–	–	–	–	–
5	(360) 364	(400) 398	–	–	–	–
	(464) 480	–	–	–	–	–
19[c]	322	–	–	–	–	–
	500	–	–	–	–	–
20[c]	318	–	–	–	–	–
20[d]	339					474
						893
21[c]	304	–	–	–	–	–
22[d]	299	–	–	–	–	336
23[d]	382	–	–	–	–	495
						909

[a] Values measured in MeCN are reported in brackets whereas those measured in 0.1 M Bu_4NPF_6/CH_2Cl_2 are without brackets. [b] Assignments **A**–**F** do not apply to complexes **19**–**23**; for these, the most intense neutral Ru^{II} (**A**) and radical cation Ru^{III} (**F**) absorptions are reported. [c] Ref. [13b]. [d] Selected values are adapted to nm from cm^{-1} and were measured in 0.1 M Bu_4NPF_6/CH_2Cl_2; Ref. [21].

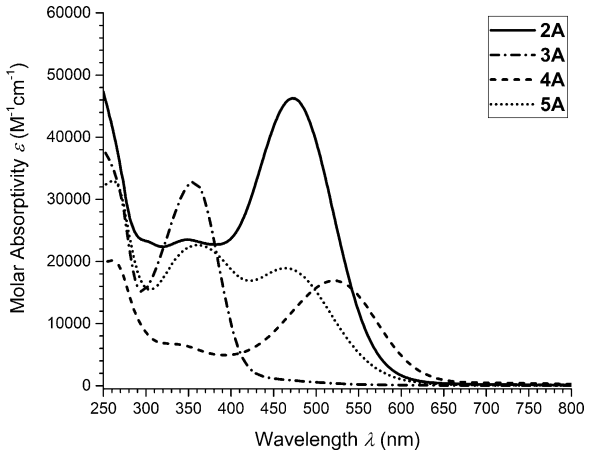

Figure 7. UV/Vis spectra of [Ru*]–DHA dyads **2A**–**5A** in MeCN.

a combination of such processes. Notably, the *meta*-coupling of complex **3A** seems to greatly weaken the interaction of the Ru metal center with the DHA fragment. The most redshifted absorption is exhibited by complex **4A**, where the [Ru*]–alkynyl group is directly attached to the DHA core.

It is also notable that upon oxidation from Ru^{II} to Ru^{III}, complexes **20** and **22**–**23** systematically present redshifted UV/Vis absorption maxima corresponding to a Ru^{III} alkynyl system. In contrast to this, oxidation product **2F** presents a blueshifted absorption maximum analogous to vinylidene **2B** and similar to **3B**–**5B** as well. This indicates strong structural similarities between the chromophoric systems of these complexes, which is reasonable as we would expect dimer **2F**, for steric reasons, to exhibit characteristics of two non-interacting (out of plane) vinylidene units.

The NMR (upfield ^{31}P-shifts), IR (Ru=C=C stretches), electrochemical (redox behavior), and UV/Vis (blueshifted absorption maxima) data strongly suggest that **2F** exhibits a vinylidene-like structure and properties. These observations are in good accord with the hypothesized dimerization mechanism, and with the proposed divinylidene [Ru*]–DHA dimer **2F** (Figure 8). Similar dimerization phenomena have previously been observed for analogous Ru and other metal complexes.[22] In particular, the aforementioned divinylidene $[\{Cp(PPh_3)_2Ru\}_2(\mu\text{-}C_4Ph_2)][PF_6]_2$, isolated by Bruce et al. by treatment of $Cp(PPh_3)_2RuC_2Ph$ with AgC_2Ph,[23] presents an analogous structure to that hypothesized for **2F**.

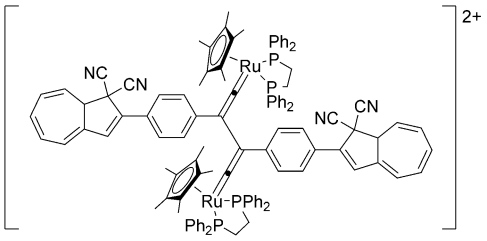

Figure 8. Hypothesized structure of [Ru*]–DHA dimer **2F**.

Multimode switching studies

Each of the [Ru*]–DHA conjugates were subjected to detailed photoswitching experiments by using UV/Vis absorption spectroscopy to follow the conversions. Full, six-state switching was successfully achieved for [Ru*]–DHA complex **2A** by using redox, acid/base, light, and thermal stimulation (Scheme 8). However, although each individual state could be achieved in one or more steps, the outcome of the light stimulus depended on the state of the Ru moiety.

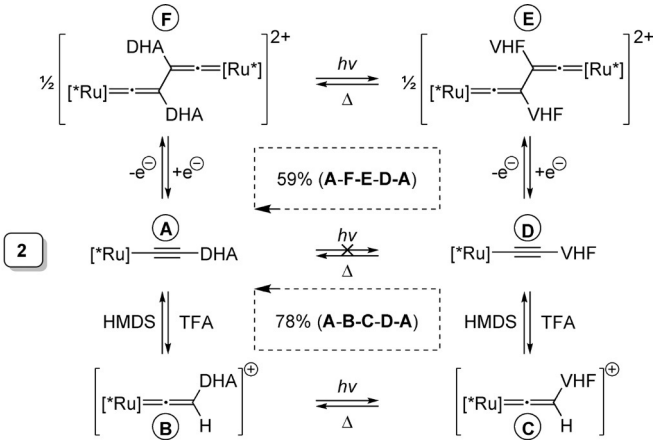

Scheme 8. Conversion between the six states of [Ru*]–DHA complex **2A** The numbers inside the dotted boxes indicate the percentage regeneration of the initial state (**A**) after a cycle of the type **A**→**B**→**C**→**D**→**A** or **A**→**F**→**E**→**D**→**A**.

The studies were conducted according to two methods. Redox chemistry was performed in an optically transparent thin layer electrochemical (OTTLE) cell having an approximately 0.2 mm path length in CH_2Cl_2 by using Bu_4NPF_6 as the supporting electrolyte. On the other hand, acid/base chemistry was performed in a Schlenk-adapted UV cuvette with a path length of 1 cm by using MeCN as the solvent. The spectroscopic results of the multimode switching experiments on **2A** are summarized in Figure 9.

A direct photoinduced ring-opening of **2A** to **2D** did not proceed and may be rationalized by quenching of the photoexcited state by interaction with the metal center.[12b] This has previously been observed in DHA systems incorporating functional groups such as anthraquinone,[12c] ferrocene,[12b] tetrathiafulvalene,[12f] amines,[12d,g,h] and C_{60}[12j] and is presumably either a result of light-induced electron transfer involving the redox-active unit or electronic perturbation of the DHA chromophore. Alternatively, the cross-conjugated system of **3A** did in fact allow photochemical isomerization to **3D**; however, with a much lower photoactivity (see the Supporting Information, p. S65) compared with reference DHA **1A**.[25] Both the electrochemical oxidation of Ru^{II} to Ru^{III} (**2A** to **2F**) and protonation of the acetylide to the vinylidine (**2A** to **2B**) were successful. In each case, the electronic communication across the acetylide bridge has been altered and the strong electron-donating power of the Ru metal center into the DHA core is effectively turned off. As the resulting chromophores are presumed to be structurally similar, it is not surprising to observe strong similarities in the UV/Vis absorption spectra of **2B** and **2F** (Figure 9).

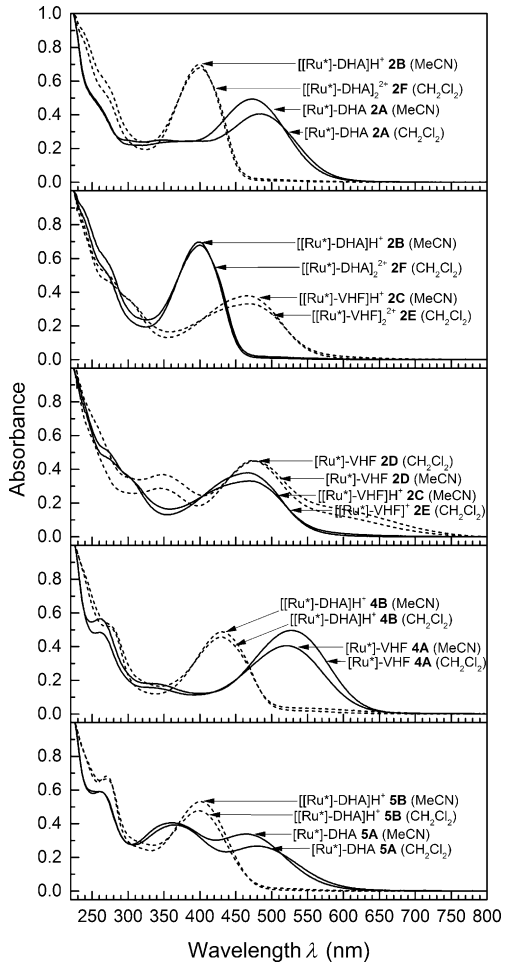

Figure 9. Normalized UV/Vis spectra ($A_{226nm} = 1$) illustrating the multiple states of [Ru*]–DHA dyads **2A**, **4A**, and **5A**. Spectra of states in MeCN were generated by chemical stimulation (acid/base) and acquired in a UV cuvette, whereas spectra of states in CH_2Cl_2 were generated by electrochemical stimulation in a 0.1 M Bu_4NPF_6/CH_2Cl_2 medium and acquired in an OTTLE cell (see the Supporting Information, Section 4).

Thus, protonation or oxidation of **2A** was found to re-establish the photoactivity of the DHA system. Photochemical isomerization of both **2B** to **2C** and **2F** to **2E**, could be accomplished by irradiation at their respective absorption maxima. It was also observed that **2C** and **2E** present analogous features in their UV/Vis absorption spectra, again suggesting structurally analogous chromophoric features. Although the initial electrochemical oxidation product of **2A** can be assigned to the hypothesized dimeric structure **2F**, the subsequent photoswitching process and structural assignment of state **2E** is only based on UV/Vis characterization.

Finally, stimulation of either **2F** by reduction or of **2B** by deprotonation leads to the formation of **2D**, which in both cases exhibits the same two absorption maxima as well as a characteristically broad shoulder ($\lambda_{max} = 600$ nm) in the UV/Vis absorption spectrum (Figure 9). In both cases, **2D** thermally reverts to **2A**, completing the cycle. The regeneration of **2A** proceeds in 78% and 59% yield for the acid/base and electrochemical cycles, respectively (illustrated in Scheme 8).

Although the acid/base switching experiments were conducted in an excess of these reactants, neither the photochemical ring-opening nor the thermal ring-closure is expected to be affected by these conditions. Previous studies have indeed demonstrated this for DHA **1A** and others.[12g,26]

Overall, six states of switching have been achieved for [Ru*]–DHA conjugate **2A**. Not surprisingly, several of these resemble each other in their UV/Vis absorption spectra even though they were reached by fundamentally different pathways.

[Ru*]–DHA conjugates **3A**, **4A**, and **5A** did not exhibit the same degree of switchability as complex **2A**. It was found that electrochemical oxidation of these complexes in fact resulted in the quantitative formation of vinylidene species **3B**–**5B** (see the Supporting Information, Section 5). Complex **3B** could thus be generated from **3A** by protonation (see the Supporting Information, p. S66), or under electrochemically oxidizing conditions. Furthermore, **3A** was found to be photoactive in both neutral and protonated (**3B**) forms, thus convertible to **3D** and **3C**, respectively. States **3C** and **3D** could subsequently be interconverted by either acid/base or electrochemical stimulation. A maximum of four states could thus be achieved for complex **3A** (Scheme 9).

Complex **4A** could only be stimulated to quantitatively achieve a maximum of two states (Scheme 9). Conversion of **4A** to vinylidene **4B** could be achieved by chemical (see the Supporting Information, p. S71) and electrochemical methods (see the Supporting Information, Section 5). In the case of **4A**, electrochemical oxidation also resulted in features in the UV/

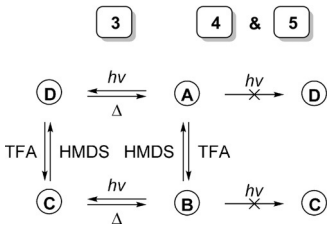

Scheme 9. Multimode switching behavior of [Ru*]–DHA conjugates **3A**, **4A**, and **5A**.

Vis absorption spectra that might be assigned to a Ru^{III} radical cation, but this was not investigated in more detail (see the Supporting Information, p. S88). Photochemical isomerization of **4A** to **4D** was unfortunately unsuccessful, as was that of **4B** to **4C**. Complex **5A** behaved analogously to **4A** (Figure 9). The protonation of [Ru*]–DHA conjugates **2A**–**5A** was, in all cases, accompanied by clear color changes as shown in Figure 10. Table 6 summarizes the UV/Vis absorption data for the achievable states of each system (**2A**–**5A**) as well as reference compounds **1A** and **19**–**21**.

Conclusions

The synthesis and characterization of four organometallic [Ru*]–DHA photoswitches (**2A**–**5A**) was accomplished. The coupling of the ruthenium and DHA motifs in the last synthetic step was found to be more reliably conducted through a metalation reaction rather than a Sonogashira cross-coupling reaction. For the two complexes where the intended 7-substituted isomers were the desired outcome (**4A**, **5A**), the metalation route instead led to the 6-substituted products as well as a few unexpected complexes, some of which were identified by single-crystal X-ray diffraction crystal structure determination.

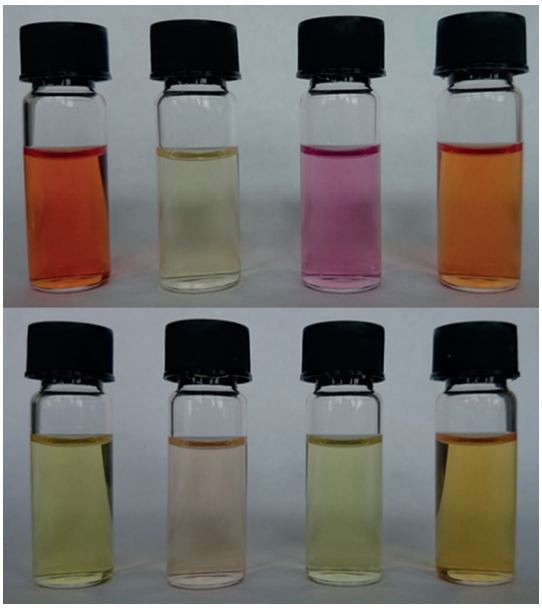

Figure 10. From left to right: Solutions of **2A**, **3A**, **4A**, and **5A** (top) and protonated complexes **2B**, **3B**, **4B**, and **5B** (bottom) (ca. 6×10^{-5} M in MeCN).

Complexes **2A**–**5A** were studied to determine the effect and functionality of the ruthenium metal center on the properties of the DHA system and vice versa. Results from spectroscopic interpretations indicate significant metal–ligand interactions between these two moieties compared with reference and literature values. This could be seen not only from their UV/Vis absorption spectra, but also by crystallographic (lengthening of C≡C bonds), IR (lowering of ν(C≡C) energy), and ^{13}C NMR (downfield shift of the [Ru*]–C triplet) spectroscopic studies. As the magnitude of these interactions increases, the complexes exhibit intense UV/Vis absorptions with increasingly redshifted absorption maxima.

Incorporation of the ruthenium acetylide moiety at varying positions on the DHA core was found to have a great effect on the light-induced photoswitching of the DHA to VHF, effectively quenching the ring-opening isomerization for complexes **2A**, **4A**, and **5A** in the neutral state. Interestingly, when attenuating the electronic interaction through a *meta*-phenylene bridge, the photoactivity was maintained (complex **3A**). In regard to the influence of cross-conjugation, it has previously been observed that the kinetics of the VHF ring-closure reaction are significantly less influenced by an electron-accepting group when placed in cross-conjugation to the VHF compared with direct linear conjugation.[27]

Electrochemical and spectroelectrochemical studies employing cyclic voltammetry and UV/Vis absorption spectroscopy support the full six-state switching potential of complex **2A**, whereas only four distinct and interconvertible states could be obtained for **3A**, and just two could be assigned for **4A** and **5A**. Oxidation of **2A** is thought to transiently form the Ru^{III} radical cation, which subsequently dimerizes to species **2F**.

Experimental Section

Unless otherwise stated, all reactions and manipulations of air- and moisture-sensitive materials were performed under an argon or nitrogen atmosphere, with all glassware having been pre-dried in an oven at 200 °C overnight or flame-dried prior to use. No special precautions to exclude air or water were taken during the subsequent workup procedures, which were conducted under atmospheric conditions. All light-sensitive compounds, reactions, and manipulations were excluded from light by either conducting the procedures in a very dimly lit room, at night, or by masking the glassware and equipment with aluminum foil. Common solvents were dried and degassed prior to use (see the Supporting Information, p. S2).

All commercially available reagents were used as received without further purification. Nuclear magnetic resonance (NMR) spectra were acquired with either a Bruker Ultrashield Plus 500 (^{1}H at 500 MHz, ^{13}C at 126 MHz) or a 500 MHz Varian spectrometer (^{1}H at 500 MHz, ^{31}P at 202 MHz), the former was equipped with a non-inverse cryoprobe. Chemical shift values are provided relative to internal solvent references for ^{1}H and ^{13}C NMR spectra and an internal reference tube containing H_3PO_4 ($\delta = 0.00$ ppm) for ^{31}P NMR spectra. Infrared spectroscopy (IR) data was acquired with a Bruker Alpha FTIR spectrometer, equipped with ALPHA's Platinum ATR single-reflection diamond ATR module instrument. Samples were

loaded directly or by evaporation from a suitable solvent. IR absorptions are reported in units of wavenumbers (cm^{-1}). UV/Vis absorption methods are detailed in the Supporting Information (Section 4). Thermal ellipsoid plots of individual molecules were generated by using Mercury 1.4.2 for Windows. Thin layer chromatography (TLC) was conducted by using commercially available, precoated plates (silica 60) with a fluorescence indicator. With respect to the DHA compounds, TLC was carried out in the absence of light, and where a color change from yellow to red upon exposure to UV light indicates a conversion to VHF. All melting points are uncorrected. CCDC 1434224 (**2 A**), 1434949 (**4 A**), 1434948 (**16**), and 1434954 (**18**) contain the supplementary crystallographic data for this paper. These data are provided free of charge by The Cambridge Crystallographic Data Centre.

Acknowledgments

The University of Copenhagen is acknowledged for financial support.

Keywords: acetylides · azulenes · fulvenes · organometallic compounds · photochromism

[1] a) A. R. Pease, J. O. Jeppesen, J. F. Stoddart, Y. Luo, C. P. Collier, J. R. Heath, *Acc. Chem. Res.* **2001**, *34*, 433 – 444; b) A. Troisi, M. A. Ratner, *Small* **2006**, *2*, 172 – 181; c) N. Weibel, S. Grunder, M. Mayor, *Org. Biomol. Chem.* **2007**, *5*, 2343 – 2353; d) R. Klajn, J. F. Stoddart, B. A. Grzybowski, *Chem. Soc. Rev.* **2010**, *39*, 2203 – 2237; e) S. Jan van der Molen, P. Liljeroth, *J. Phys. Condens. Matter* **2010**, *22*, 133001; f) S. J. van der Molen, P. Liljeroth, *Conductance Properties of Switchable Molecules, in Molecular Switches, Vol. 2* (Eds.: B. L. Feringa, W. R. Browne), Wiley-VCH, Weinheim, **2011**, pp. 719 – 777; g) S. L. Broman, M. B. Nielsen, *Phys. Chem. Chem. Phys.* **2014**, *16*, 21172 – 21182; h) D. Kim, H. Jeong, H. Lee, W. T. Hwang, J. Wolf, E. Scheer, T. Huhn, H. Jeong, T. Lee, *Adv. Mater.* **2014**, *26*, 3968 – 3973.

[2] a) J. Andréasson, U. Pischel, *Chem. Soc. Rev.* **2010**, *39*, 174 – 188; b) A. P. de Silva, T. P. Vance, B. Wannalerse, M. E. S. West, *Molecular Logic Systems, in Molecular Switches, Vol. 2* (Eds.: B. L. Feringa, W. R. Browne), Wiley-VCH, Weinheim, **2011**, pp. 669 – 696.

[3] B. J. Coe, *Chem. Eur. J.* **1999**, *5*, 2464 – 2471.

[4] F. Pina, A. J. Parola, R. Gomes, M. Maestri, V. Balzani, *Multistate/Multifunctional Molecular-Level Systems: Photochromic Flavylium Compounds, in Molecular Switches, Vol. 1* (Eds.: B. L. Feringa, W. R. Browne), Wiley-VCH, Weinheim, **2011**, pp. 181 – 226.

[5] M. Akita, *Organometallics* **2011**, *30*, 43 – 51.

[6] J. Manna, K. D. John, M. D. Hopkins, *Adv. Organomet. Chem.* **1995**, *38*, 79 – 154.

[7] a) B. Li, J.-Y. Wang, H.-M. Wen, L.-X. Shi, Z.-N. Chen, *J. Am. Chem. Soc.* **2012**, *134*, 16059 – 16067; b) H.-M. Wen, B. Li, J.-Y. Wang, L.-X. Shi, C.-N. Chen, Z.-N. Chen, *Organometallics* **2013**, *32*, 1759 – 1765; c) Y. Liu, C. M. Ndiaye, C. Lagrost, K. Costuas, S. Choua, P. Turek, L. Norel, S. Rigaut, *Inorg. Chem.* **2014**, *53*, 8172 – 8188.

[8] a) Y. Tanaka, T. Ishisaka, A. Inagaki, T. Koike, C. Lapinte, M. Akita, *Chem. Eur. J.* **2010**, *16*, 4762 – 4776; b) Y. Lin, H. Cui, P. Wan, J. Yin, S. Liu, *Mol. Cryst. Liq. Cryst.* **2015**, *608*, 55 – 61.

[9] K. A. Green, M. P. Cifuentes, T. C. Corkery, M. Samoc, M. G. Humphrey, *Angew. Chem. Int. Ed.* **2009**, *48*, 7867 – 7870; *Angew. Chem.* **2009**, *121*, 8007 – 8010.

[10] F. Meng, Y.-M. Hervault, L. Norel, K. Costuas, C. Van Dyck, V. Geskin, J. Cornil, H. H. Hng, S. Rigaut, X. Chen, *Chem. Sci.* **2012**, *3*, 3113 – 3118.

[11] a) S. Lara-Avila, A. V. Danilov, S. E. Kubatkin, S. L. Broman, C. R. Parker, M. B. Nielsen, *J. Phys. Chem. C* **2011**, *115*, 18372 – 18377; b) S. L. Broman, S. Lara-Avila, C. L. Thisted, A. D. Bond, S. Kubatkin, A. Danilov, M. B. Nielsen, *Adv. Funct. Mater.* **2012**, *22*, 4249 – 4258; c) T. Li, M. Jevric, J. R. Hauptmann, R. Hviid, Z. Wei, R. Wang, N. E. A. Reeler, E. Thyrhaug, S. V. Petersen, J. A. S. Meyer, N. E. Bovet, T. A. J. Vosch, J. Nygård, X. Qiu, W. Hu, Y. Liu, G. C. Solomon, H. G. Kjaergaard, T. Bjørnholm, M. B. Nielsen, M. W. Laursen, K. Nørgaard, *Adv. Mater.* **2013**, *25*, 4164 – 4170.

[12] a) J. Daub, J. Salbeck, T. Knöchel, C. Fischer, H. Kunkely, K. M. Rapp, *Angew. Chem. Int. Ed. Engl.* **1989**, *28*, 1494 – 1496; *Angew. Chem.* **1989**, *101*, 1541 – 1542; b) J. Daub, S. Gierisch, J. Salbeck, *Tetrahedron Lett.* **1990**, *31*, 3113 – 3116; c) J. Achatz, C. Fischer, J. Salbeck, J. Daub, *J. Chem. Soc. Chem. Commun.* **1991**, 504 – 507; d) L. Gobbi, P. Seiler, F. Diederich, *Helv. Chim. Acta* **2001**, *84*, 743 – 777; e) M. Å. Petersen, L. Zhu, S. H. Jensen, A. S. Andersson, A. Kadziola, K. Kilså, M. B. Nielsen, *Adv. Funct. Mater.* **2007**, *17*, 797 – 804; f) M. Å. Petersen, A. S. Andersson, K. Kilså, M. B. Nielsen, *Eur. J. Org. Chem.* **2009**, 1855 – 1858; g) S. L. Broman, M. Å. Petersen, C. G. Tortzen, A. Kadziola, K. Kilså, M. B. Nielsen, *J. Am. Chem. Soc.* **2010**, *132*, 9165 – 9174; h) M. Å. Petersen, S. L. Broman, K. Kilså, A. Kadziola, M. B. Nielsen, *Eur. J. Org. Chem.* **2011**, 1033 – 1039; i) L. Skov, M. Å. Petersen, S. L. Broman, A. D. Bond, M. B. Nielsen, *Org. Biomol. Chem.* **2011**, *9*, 6498 – 6501; j) M. Santella, V. Mazzanti, M. Jevric, C. R. Parker, S. L. Broman, A. D. Bond, M. B. Nielsen, *J. Org. Chem.* **2012**, *77*, 8922 – 8932; k) S. L. Broman, M. Jevric, M. B. Nielsen, *Chem. Eur. J.* **2013**, *19*, 9542 – 9548.

[13] a) C. Bitcon, M. W. Whiteley, *J. Organomet. Chem.* **1987**, *336*, 385 – 392; b) F. Paul, B. G. Ellis, M. I. Bruce, L. Toupet, T. Roisnel, K. Costuas, J. F. Halet, C. Lapinte, *Organometallics* **2006**, *25*, 649 – 665.

[14] K. Sonogashira, Y. Tohda, N. Hagihara, *Tetrahedron Lett.* **1975**, *16*, 4467 – 4470.

[15] M. I. Bruce, B. G. Ellis, P. J. Low, B. W. Skelton, A. H. White, *Organometallics* **2003**, *22*, 3184 – 3198; b) M. I. Bruce, M. A. Fox, P. J. Low, B. K. Nicholson, C. R. Parker, W. C. Patalinghug, B. W. Skelton, A. H. White, *Organometallics* **2012**, *31*, 2639 – 2657.

[16] S. L. Broman, M. Jevric, A. D. Bond, M. B. Nielsen, *J. Org. Chem.* **2014**, *79*, 41 – 64.

[17] S. L. Broman, S. L. Brand, C. R. Parker, M. Å. Petersen, C. G. Tortzen, A. Kadziola, K. Kilså, M. B. Nielsen, *Arkivoc* **2011**, *4*, 51 – 67.

[18] For a recent account of the synthesis and functionalization of DHA, see: M. Cacciarini, S. L. Broman, M. B. Nielsen, *Arkivoc* **2014**, *1*, 249 – 263.

[19] a) P. M. Treichela, D. A. Komara, P. J. Vincentia, *Synth. React. Inorg. Met. – Org. Chem.* **1984**, *14*, 383 – 400; b) F. Morandini, A. Dondana, I. Munari, G. Pilloni, G. Consiglio, A. Sironi, M. Moret, *Inorg. Chim. Acta* **1998**, *282*, 163 – 172.

[20] D. Pilette, K. Ouzzine, H. Le Bozec, P. H. Dixneuf, C. E. F. Rickard, W. R. Roper, *Organometallics* **1992**, *11*, 809 – 817.

[21] M. A. Fox, R. L. Roberts, W. M. Khairul, F. Hartl, P. J. Low, *J. Organomet. Chem.* **2007**, *692*, 3277 – 3290.

[22] a) R. S. Iyer, J. P. Selegue, *J. Am. Chem. Soc.* **1987**, *109*, 910 – 911; b) S. Rigaut, F. Monnier, F. Mousset, D. Touchard, P. H. Dixneuf, *Organometallics* **2002**, *21*, 2654 – 2661; c) D. A. Valyaev, O. V. Semeikin, N. A. Ustynyuk, *Coord. Chem. Rev.* **2004**, *248*, 1679 – 1692; d) M. I. Bruce, B. G. Ellis, B. W. Skelton, A. H. White, *J. Organomet. Chem.* **2005**, *690*, 792 – 801; e) M. I. Bruce, B. G. Ellis, B. W. Skelton, A. H. White, *J. Organomet. Chem.* **2005**, *690*, 1772 – 1783; f) N. A. Ustynyuk, O. V. Gusev, L. N. Novikova, M. G. Peterleitner, L. I. Denisovich, T. A. Peganova, O. V. Semeikin, D. A. Valyaev, *J. Solid State Electrochem.* **2007**, *11*, 1621 – 1634; g) M. A. Fox, J. D. Farmer, R. L. Roberts, M. G. Humphrey, P. J. Low, *Organometallics* **2009**, *28*, 5266 – 5269; h) M. I. Bruce, A. Burgun, F. Gendron, G. Grelaud, J.-F. Halet, B. W. Skelton, *Organometallics* **2011**, *30*, 2861 – 2868; i) P. A. Schauer, P. J. Low, *Eur. J. Inorg. Chem.* **2012**, 390 – 411; j) P. J. Low, S. Bock, *Electrochim. Acta* **2013**, *110*, 681 – 692.

[23] M. I. Bruce, G. A. Koutsantonis, M. J. Liddell, E. R. T. Tiekink, *J. Organomet. Chem.* **1991**, *420*, 253 – 269.

[24] a) K. Costuas, F. Paul, L. Toupet, J.-F. Halet, C. Lapinte, *Organometallics* **2004**, *23*, 2053 – 2068; b) R. Denis, L. Toupet, F. Paul, C. Lapinte, *Organometallics* **2000**, *19*, 4240 – 4251.

[25] H. Goerner, C. Fischer, S. Gierisch, J. Daub, *J. Phys. Chem.* **1993**, *97*, 4110 – 4117.

[26] C. R. Parker, C. G. Tortzen, S. L. Broman, M. Schau-Magnussen, K. Kilså, M. B. Nielsen, *Chem. Commun.* **2011**, *47*, 6102 – 6104.

[27] K. Fjelbye, T. N. Christensen, M. Jevric, S. L. Broman, A. U. Petersen, A. Kadziola, M. B. Nielsen, *Eur. J. Org. Chem.* **2014**, 7859 – 7864.

Received: January 14, 2016
Published online on April 26, 2016